Geophysical Research Letters

RESEARCH LETTER
10.1029/2020GL088384

Simulation of Deep Cycle Turbulence by a Global Ocean General Circulation Model

Suyang Pei[1], Toshiaki Shinoda[1], Wanqiu Wang[2], and Ren-Chieh Lien[3]

[1]Department of Physical and Environmental Sciences, Texas A&M University-Corpus Christi, Corpus Christi, TX, USA, [2]Climate Prediction Center, NOAA/NWS/NCEP, College Park, MD, USA, [3]Applied Physics Laboratory, University of Washington, Seattle, WA, USA

Key Points:
- Deep cycle turbulence is well simulated for the first time by a global ocean general circulation model in all equatorial ocean basins
- Large-scale zonal and meridional variations of the deep cycle turbulence in equatorial Pacific and Atlantic are fully described
- Separation of deep cycle turbulence from the surface mixed layer is most prominent in the central Pacific near the dateline

Supporting Information:
- Supporting Information S1

Correspondence to:
S. Pei,
suyang.pei@tamucc.edu

Citation:
Pei, S., Shinoda, T., Wang, W., & Lien, R.-C. (2020). Simulation of deep cycle turbulence by a global ocean general circulation model. *Geophysical Research Letters*, *47*, e2020GL088384. https://doi.org/10.1029/2020GL088384

Received 15 APR 2020
Accepted 13 JUL 2020
Accepted article online 17 JUL 2020

Abstract Deep cycle turbulence (DCT) is a diurnally oscillating turbulence that penetrates into a stratified shear layer below the surface mixed layer, which is often observed in the eastern Pacific and Atlantic above the Equatorial Undercurrent (EUC). Here we present the simulation of DCT by a global ocean general circulation model (OGCM) for the first time. As the k-ε vertical mixing scheme is used in the OGCM, the simulation of observed DCT structure based on in situ microstructure measurements can be explicitly demonstrated. The simulated DCT is found in all equatorial ocean basins, and its characteristics agree very well with observations. Zonal and meridional variations of DCT in the entire equatorial Pacific and Atlantic are described through constructing the composite diurnal cycle. In the central Pacific where the maximum shear associated with EUC is deep, the separation of DCT from the surface mixed layer is much more prominent than other areas.

Plain Language Summary Deep cycle turbulence (DCT) is a nighttime intensified turbulence that develops in the stratified layer below the base of the surface mixed layer. It is often observed below the equatorial Pacific and Atlantic cold tongue regions above the Equatorial Undercurrent (EUC). Mixing caused by DCT is essential in modulating sea surface temperature (SST), which could have a large impact on air-sea interaction and thus global climate variability. However, simulations of DCT in global ocean models have not been demonstrated so far, and the spatial variation of DCT characteristics in the entire equatorial oceans is not well known. This study presents the first global ocean general circulation model simulation of DCT, demonstrated by the comparison of simulated turbulence with that derived from in situ observations. The simulated DCT is found in all equatorial ocean basins, and its characteristics agree very well with observations. Large-scale spatial variability of DCT in the equatorial Pacific and Atlantic is described through the analysis of model output. The DCT layer completely separated from surface mixed layer is found at locations where the EUC is deep, such as the central equatorial Pacific near the dateline.

1. Introduction

Deep cycle turbulence (DCT) is a nighttime intensified turbulence that extends below the base of the surface mixed layer (SML). It has been often observed below the equatorial Pacific and Atlantic cold tongue regions above the Equatorial Undercurrent (EUC). Despite the ongoing debate on the triggering mechanism (Pham et al., 2012, 2013, 2017; Smyth et al., 2013), DCT develops in a stratified shear layer with the mean flow at a state of marginal instability (MI) (Pham et al., 2013; Smyth & Moum, 2013; Thorpe & Liu, 2009). MI is a near unstable state of the mean flow indicated by a critical Richardson number of 1/4. Maintaining MI state is an essential characteristic of DCT (Smyth & Moum, 2013; Smyth et al., 2019).

Since the discovery of DCT in 1980s (Gregg et al., 1985; Moum & Caldwell, 1985), it has been extensively studied over decades because of its essential role in modulating the sea surface temperature (SST) in the eastern equatorial Pacific (Moum et al., 2009, 2013), which could have a strong impact on air-sea interaction and thus global climate variability (e.g., Huang et al., 2013; Kosaka & Xie, 2013; Warner & Moum, 2019; Xie, 2013). Hence, an adequate parameterization of DCT may reduce the SST bias in the Pacific cold tongue persistently evident in coupled general circulation models (e.g., de Szoeke & Xie, 2008; Li & Xie, 2014; Richter et al., 2016; Samanta et al., 2019; Zheng et al., 2012).

Most studies of DCT so far are based on in situ measurements on the equator in the eastern Pacific and Atlantic (e.g., Hebert et al., 1991; Hummels et al., 2013; Inoue et al., 2012, 2019; Lien et al., 1995, 1996,

2008; Moum et al., 1989, 1992, 2009, 2013; Peters et al., 1988; Smyth & Moum, 2013; Smyth et al., 2013, 2017, 2019; Warner & Moum, 2019; Wenegrat & McPhaden, 2015), while only few modeling studies on DCT have been reported (Clayson & Kantha, 1999; Pham et al., 2012, 2013, 2017; Schudlich & Price, 1992; Wang et al., 1998). While recent studies using regional ocean general circulation models (OGCMs) in the tropical Pacific suggest the possible modulation of DCT by tropical instability waves (TIWs) (Holmes & Thomas, 2015; Inoue et al., 2019), DCT in the simulations is not explicitly presented in these studies and thus OGCM's ability to simulate DCT is still unknown. Accordingly, large-scale spatial variations of DCT, which require its full description over the equatorial ocean basins, have not been reported yet.

This work presents the first global OGCM simulation of DCT, which agrees very well with observations. Since a k-ε model based second-moment turbulence closure is used for the vertical mixing parameterization in the OGCM, the simulated turbulent kinetic energy (TKE) dissipation rate ε is directly compared with that obtained from the in situ microstructure measurements. Model results are validated against the observational data to demonstrate its ability to simulate the diurnally varying turbulence. As the global model is used, the spatial variations of DCT characteristics can be fully described. The analysis of the model simulation indicates that simulated DCTs are evident in all equatorial ocean basins with their MI state being well reproduced. In addition, processes that control the modulation of DCT simulated by the model, including the role of TIWs, are consistent with previous studies. A special emphasis is given to the DCTs in the equatorial Pacific and Atlantic, where their zonal and meridional variations are discussed in detail. In particular, the vertical structure of turbulence is shown to vary substantially with the longitude in the equatorial Pacific because of the zonal variation of EUC depth.

2. OGCM Simulation

The OGCM used in this study is a Geophysical Fluid Dynamics Laboratory (GFDL)'s Modular Ocean Model, Version 5 (MOM5; Griffies, 2012) for the global domain with some modifications from the original version. These modifications include the implementation of the Coupled Ocean-Atmosphere Response Experiment bulk flux algorithm (COARE 3.5; Edson et al., 2013; Fairall et al., 2003) and the General Ocean Turbulence Model (GOTM; Burchard et al., 1999; Umlauf et al., 2005).

The model grids are similar to Ge et al. (2017), in which the zonal resolution is 0.5° and the meridional resolution is 0.25° between 10°S and 10°N, gradually increasing poleward to 0.5° at 30°S and 30°N and fixed beyond. A 50-layer z^* coordinate is used in the vertical direction. The layer thickness is 1 m for the upper 9 m, gradually increasing to 10 m at 40 m and constant up to 220 m. Then it increases toward the bottom of the ocean. The model is driven by hourly atmospheric forcing created by Ge et al. (2017) which is based on the 1-hr outputs from the Climate Forecast System Reanalysis (CFSR; Saha et al., 2010) and the Modern-Era Retrospective Analysis for Research and Applications (MERRA; Rienecker et al., 2011). Note that many previous OGCM simulations to study equatorial turbulence (e.g., Holmes & Thomas, 2015; Inoue et al., 2019) did not use hourly forcing, and thus, DCT cannot be generated in those simulations.

To parameterize the vertical mixing process, we use the second-moment turbulence closure developed by Canuto et al. (2001). The turbulence length scale is calculated by the k-ε model (Burchard & Bolding, 2001; Rodi, 1987). Since ε is explicitly calculated at each time step during the model integration, it can be compared directly with that derived from microstructure measurements. The model is integrated from 1 September to 31 December 2011 with initial conditions taken from the oceanic state of the CFSR (Ge et al., 2017). The hourly model outputs are analyzed.

The simulated temperature and velocity are compared with in situ data at various locations on the equator from the TAO (McPhaden et al., 1998), PIRATA (Foltz et al., 2018), and RAMA (McPhaden et al., 2009) moorings during the analysis period, showing a reasonably good agreement with the observed vertical profiles from equatorial moorings at 80.5°E, 140°W, 35°W, and 23°W (Figures S1 and S2 in the supporting information).

3. Results

3.1. Simulated DCT in all Equatorial Ocean Basins

DCT has been observed by a number of in situ microstructure measurements in the eastern equatorial Pacific and Atlantic (e.g., Hummels et al., 2013; Moum et al., 2009). DCT, similar to previous observations

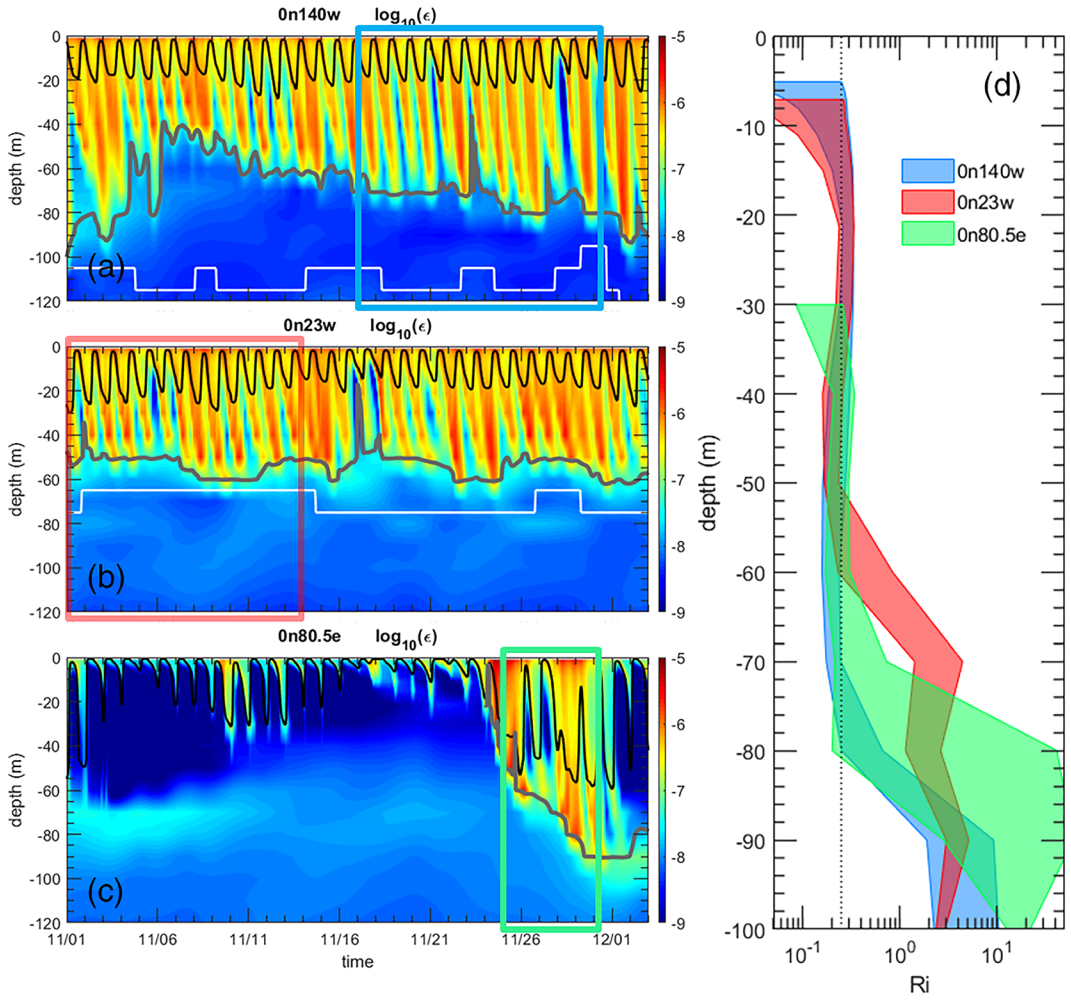

Figure 1. Time-depth contours of modeled $\log_{10}\varepsilon$ (shading), where ε is turbulence kinetic energy dissipation rate and mixed layer depth (black line) from 1 November to 3 December 2011 on the equator at (a) 140°W, (b) 23°W, and (c) 80.5°E. (d) Middle quartile (25–75%) of the time-averaged gradient Richardson number at each location during the period of 17–30 November (blue box), 1–14 November (red box), and 25–30 November (green box). Values of negative *Ri* within the mixed layer are not included in the plot. The vertical dotted line indicates $Ri = 1/4$, which is a marginal instability state often observed for DCT. Gray lines in (a)–(c) show the base of the marginal instability layer, corresponding to the deepest depth with $Ri = 1/4$. White lines in (a) and (b) represent the core of the EUC indicated by the maximum of zonal velocity.

(e.g., Smyth & Moum, 2013; Wenegrat & McPhaden, 2015), is clearly evident in present OGCM simulations shown in Figures 1a and 1b, which display time-depth variations of simulated ε in the eastern Pacific (0°, 140°W) and eastern Atlantic (0°, 23°W), respectively. The strong ε penetrates below the base of the SML, which is defined as the depth where the density exceeds its surface value by 0.01 kg m^{-3}. At 0°, 140°W, the depth of SML during nighttime is about 20 m, and the DCT penetrates to 50- to 100-m depth. The maximum depth of DCT closely follows the base of MI layer, which is often located around the upper flank of EUC. Some strong DCT events, such as those in early November and December, reach as deep as 100 m. These simulated DCT characteristics are at least qualitatively in good agreement with previous in situ microstructure measurements such as those taken during 2008 (Figure 1 in Smyth & Moum, 2013) except that the simulated ε is slightly weaker than the observation. Note that both 2008 and 2011 are La Niña years with strong TIWs and strong EUC shear in the eastern equatorial Pacific. It is worth mentioning that multiple nighttime turbulence bursts associated with DCT (Pham et al., 2017; Smyth & Moum, 2013) are occasionally found in our simulation (e.g., 1–4 November, Figure 1a). They could be due to the oscillatory interaction between the mean shear and the turbulence (Smyth et al., 2017), which can

be modeled by the mixing parameterization. The simulated bursts, however, have smaller ε variation than observations possibly due to small-scale processes (e.g., nonlinear vortices, Pham et al., 2013) which cannot be adequately resolved by the OGCM.

DCT at 0°, 23°W reaches around a depth of 60 m during the simulation period, shallower than that in the eastern Pacific because of a shallower EUC at this location (e.g., Brandt et al., 2014; Giarolla et al., 2005). The average ε over 20–50 m during this period is about 4.6×10^{-7} m^2 s^{-3}, which is consistent with observations at this location in November 2008 (Wenegrat & McPhaden, 2015). Previous observational studies conclude that the energy source of DCTs is provided by strong vertical shear of mean currents in a stratified background flow where gradient Richardson number (Ri) is close to the critical value 1/4 (MI state). The MI state similar to observations is found in the model simulations (Figure 1d). It is worth noting that a K-profile parameterization (KPP) vertical mixing scheme (Large et al., 1994), which is used in many OGCMs and climate models, cannot produce the MI state associated with DCT (Holmes & Thomas, 2015).

In addition to the persistent DCTs in the equatorial Pacific and Atlantic, the simulation also reveals DCT in the equatorial Indian Ocean (Figure 1c), which agrees very well with the microstructure measurements (Figure 5 in Pujiana et al., 2018). Pujiana et al. (2018) suggested that ε penetration below the mixed layer during late November 2011 is associated with DCT driven by the vertical shear caused by the westerly wind bursts associated with the Madden-Julian Oscillation (MJO) events (Moum et al., 2014). While wind bursts enhance the surface mixing, as shown by the substantial deepening of mixed layer depth (MLD), it also generates strong zonal currents that create vertical shear favoring the subsequent penetration of DCT. The layer of DCT penetration below the SML is thinner than that in the Pacific and Atlantic due to a deeper SML produced by strong westerly winds. Despite the different sources of vertical shear in the Indian Ocean, DCTs show similar MI state indicated by $Ri \approx 1/4$ (Figure 1d). The maximum depth of DCT agrees very well with the base of MI layer (Figures 1a–1c).

It is worth mentioning that the direct comparison during the simulation period has been performed only for the Indian Ocean case because the velocity shear that generates DCT during DYNAMO is associated with strong equatorial jet produced by westerly wind bursts (wind forced motion), which can be simulated by the OGCM reasonably well. Such direct comparisons are difficult for Pacific and Atlantic cases because of the strong influence of TIW whose phase and amplitude cannot be accurately simulated by OGCMs.

3.2. Modulation of the Simulated DCT

To further validate the model results, processes that control the DCT modulation, which are previously reported in observational studies, are examined by the analysis of model outputs. As such processes have been extensively studied at 0°, 140°W, the analysis focuses on the eastern Pacific.

Figure 2a shows the time series of ε profile and MLD at 0°, 140°W in October–November 2011 from the model simulation. Characteristics of DCT vary substantially during this period. Strong DCT occurs during early October (1–3 October) and late October to early November (19 October to 3 November) when strong ε associated with DCT penetrates into 50- to 100-m depths, whereas ε in other periods is weaker.

The strong DCT in early and late October can be explained by the modulation due to TIWs suggested in previous studies (Holmes & Thomas, 2015; Inoue et al., 2012, 2019; Lien et al., 2008; Moum et al., 2009). For example, Inoue et al. (2019) demonstrate that DCT is enhanced during the TIW phase of southward currents on the equator, which induces stronger vertical shear. During the periods of enhanced DCT in early and late October, strong southward currents are found on the equator (Figure 2d). They propagate westward along the equator with a phase speed of about 0.9 m s^{-1} (Figure S3), which is consistent with 17-day TIWs associated with mixed Rossby gravity waves (Lyman et al., 2007; Shinoda, 2010, 2012). Therefore, the enhancement of DCT in early and late October could be caused by southward currents associated with TIWs (Figures 2b and 2c), consistent with observations.

After 24 October, the meridional currents on the equator change to northward (Figure 2d). However, DCT continues to be strong until early November. This enhanced DCT could be due to the stronger subsurface vertical shear (Figure 2b) associated with the accelerating westward surface currents (Figure 2f), which could be generated by the enhancement of westward winds during this period (Figure 2e). The result is consistent with previous studies (Clayson & Kantha, 1999; Pham et al., 2017), which show the intensity of DCT can be increased by enhanced easterlies.

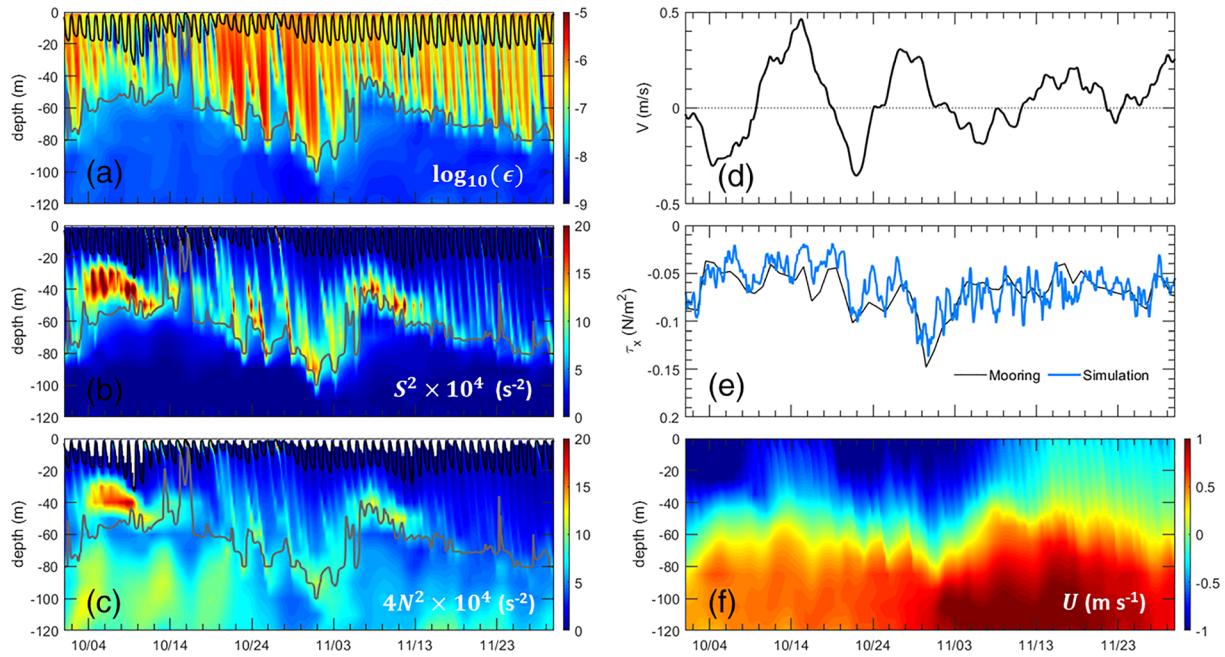

Figure 2. Time series of (a) vertical profile of $\log_{10}\varepsilon$ (shading), (b) vertical shear squared multiplied by 10^4 (shading), (c) buoyancy frequency squared multiplied by 4×10^4 (shading), (d) meridional velocity on the equator averaged over upper 30 m, (e) zonal wind stress used in the simulation (blue line) and from the TAO mooring (black thin line), and (f) vertical profile of zonal velocity on the equator at 140°W from 1 October to 30 November 2011. The black (gray) lines in panels (a)–(c) indicate mixed (MI) layer depth. The white areas in panel (c) indicate negative buoyancy frequency. Each minor tick of horizontal axis represents 2-day interval. Time series of SST and vertical profile of *Ri* are shown in Figure S3 in the supporting information.

3.3. Large-Scale Spatial Variation of DCT

3.3.1. Equatorial Pacific

Using the validated global model simulation, large-scale spatial variations of DCT are fully described. Here the spatial variation of DCT is examined by forming the composite of diurnal variation. The composite is constructed over a 4-day period (21–25 November) when the zonal wind across the equatorial Pacific was relatively steady. The diurnal variation of turbulence along the equator is shown at 3:00, 9:00, 15:00, and 21:00 GMT in Figures 3a1–3a4.

DCT is identified as strong turbulence penetrates into the stratified shear layer below the SML. The layer of DCT is defined as the layer between the daily maximum MLD and the depth of MI layer at each location. Strong DCT ($\varepsilon > 10^{-7}$ m^2 s^{-3}) with notable turbulence penetration is found on the equator between 170°E and 105°W (Figures 3a3 and 3a4) where the maximum shear is located at the upper flank of EUC (Figures S4a1–S4a4). The maximum depth of DCT gradually deepens from 105°W to 180° and then shoals toward 170°E, closely following the base of MI layer and the upper flank of EUC (Figure 3b). The strongest DCT ($\varepsilon > 10^{-6}$ m^2 s^{-3}) is found between 140°W and 110°W due to the intensified vertical shear caused by enhanced westward surface zonal currents and the shoaling of EUC. Note that the fluctuation of zonal currents along the equator (Figure 3b) is due to a modulation of TIWs.

East of 105°W, relatively weak turbulence ($\varepsilon < 10^{-7}$ m^2 s^{-3}) is confined within the upper 50 m because of intensified stratification (Figures S4c1–S4c4) caused by the upwelling (Figure S4d). In the region of 155–170°E, the layer of turbulence penetration below SML becomes thinner (~10 m) as the MI layer shoals substantially due to the weak shear and strong stratification between the deep EUC and the surface currents (Figures S4a4 and S4c4). West of 155°E, the surface zonal current is eastward (Figure 3b), and DCT does not exist.

As described above, a large zonal extent (170°E to 105°W) of DCT is evident in the model simulation. The details of diurnal variation of DCT in these regions are described in the following. At 3:00 GMT, SML starts deepening in the eastern and central Pacific when the nighttime surface cooling begins (Figure 3a1). Within the SML, strong turbulence (ε~10^{-6} m^2 s^{-3}) is found east of 180°. Below the SML, turbulence generated in

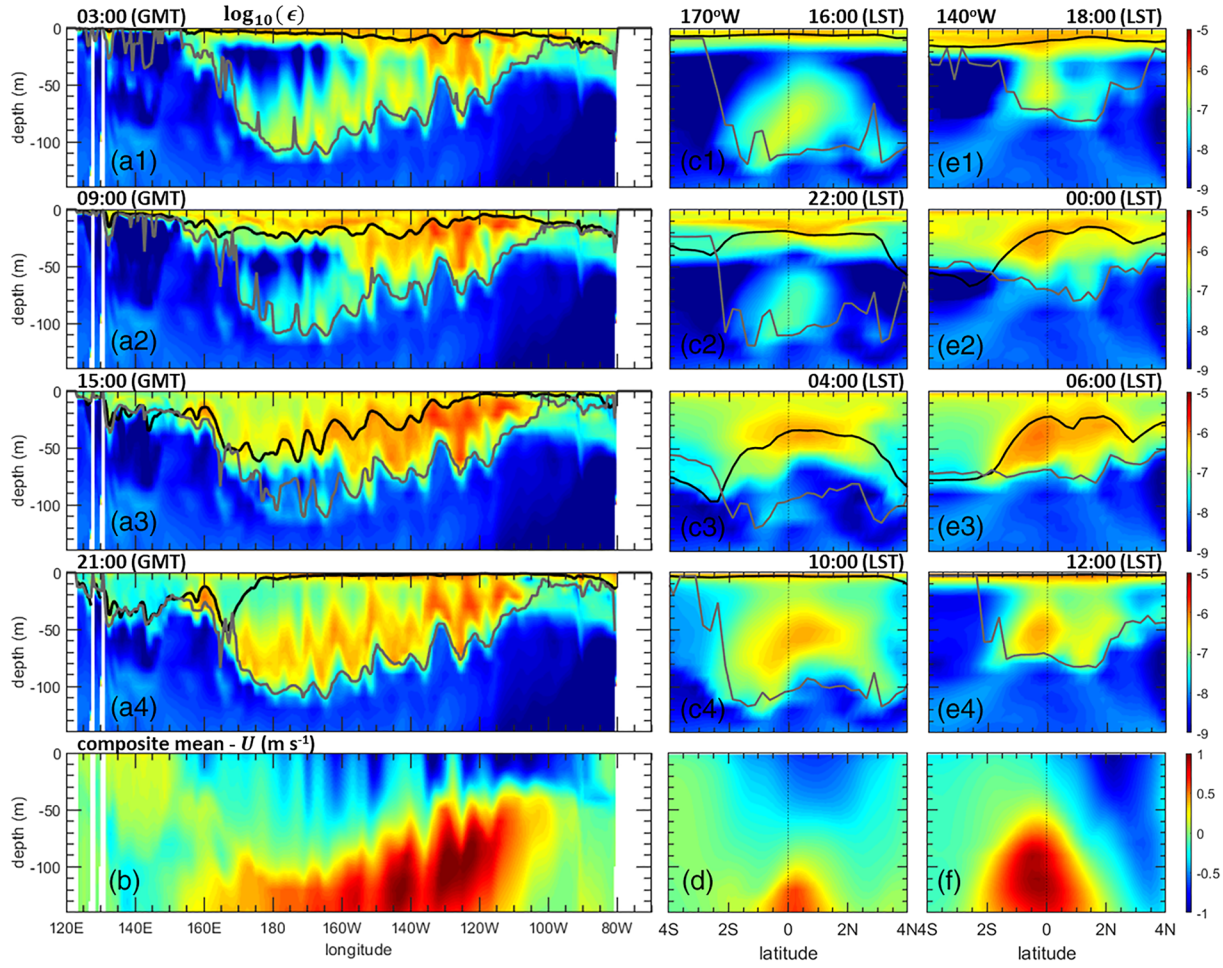

Figure 3. (a1–a4) Composite diurnal variations of $\log_{10}\varepsilon$ (shading) and MLD (black line) along the equator in the Pacific for the period 21–25 November 2011 at 03:00, 09:00, 15:00, and 21:00 GMT, respectively. (c1–c4) Same as (a1)–(a4) except at 170°W between 4°S and 4°N. (e1–e4) Same as (a1)–(a4) except at 140°W between 4°S and 4°N. (b, d, and f) The daily average of the composite zonal velocity (shading) at each location. The gray lines in panels (a), (c), (e) indicate MI layer depth. The corresponding local solar time (LST) at 170°W and 140°W is shown in (c1)–(c4) and (e1)–(e4). Variations of *Ri* and SST are shown in Figure S4 in the supporting information.

the previous night with varying intensity is evident. For instance, turbulence below the SML between 140°W and 120°W remains strong, with its intensity similar to that found in SML. In the central Pacific around 170°E to 170°W, a strong turbulence layer completely separated from the SML is found right above the upper flank of EUC. This layer corresponds to the DCT formed during the previous night, which will be explained in the following.

At 9:00 GMT, SML continues to deepen along the equator (Figure 3a2). From 170°E to 140°W, a thin turbulence layer of intensified ε (~10^{-6} m^2 s^{-3}) is noticeable right above the base of SML. This enhanced turbulence layer is found in previous observations (Lien et al., 1995; Smyth et al., 2013), which could be driven by local shear instability (Smyth et al., 2013). It is stronger than turbulence driven by nighttime convection (Figure S4c2) above this layer (Wang et al., 1998). Below SML, turbulence west of 160°W, including that in the DCT layer of previous night, continues to decay. In contrast, east of 160°W, DCT already penetrates below the base of SML as shown by higher ε than that at 3:00 GMT (Figures 3a1 and 3a2).

At 15:00 GMT, SML west of 130°W further deepens while that east of 130°W shoals in response to daytime heating (Figure 3a3). DCT becomes stronger and deeper east of 160°W as it deepens to the region of the maximum shear while SML reaching its maximum depth. West of 160°W, strong turbulence is found around the base of SML.

At 21:00 GMT, SML shoals substantially, and a very shallow mixed layer is found east of 180° because of incoming solar radiation (Figure 3a4). East of 160°W, turbulence decays due to the enhanced stratification indicated by a weaker ε than that of Figure 3a3. However, DCT remains notably strong ($\varepsilon > 10^{-7}$ m^2 s^{-3}) within the region of maximum shear (Figure S4a4). West of 160°W, the strong turbulence layer, previously found around the SML base at 15:00 GMT, keeps deepening while SML reaches its maximum depth and then shoals substantially during 15:00–21:00 GMT. This produces a strong turbulence layer above the base of MI layer as DCT penetrates into the maximum shear region. Meanwhile, turbulence below the SML at 21:00 GMT, which is previously found within the SML at 15:00 GMT, is largely suppressed as the upper ocean is restratified due to surface warming. As a result, a weak turbulence layer between the SML above and the strong DCT below is evident. Later at 3:00 GMT, this weak turbulence layer becomes remarkably weaker ($\varepsilon \leq 10^{-9}$ m^2 s^{-3}) due to further decay caused by restratification. Below this layer, DCT within the maximum shear region in the MI layer remains strong. This vertical structure of turbulence can also be viewed in the meridional sections. Along 170°W section, it is evident that the strong DCT layer left from previous turbulence penetration (Figure 3c4) is separated from SML by a weak turbulence layer (Figures 3c1 and 3c2). This weak turbulence layer disappears during 15:00–21:00 GMT and then reappears at 3:00 GMT.

Such separation of DCT from SML by a weak turbulence layer was also observed at 140°W (Lien et al., 1995; Smyth et al., 2013), and the simulated structure is consistent with the observation (Figure 3e1). However, the weak turbulence layer between SML and DCT is much more prominent and thicker around the dateline than at 140°W. This is mainly because the shallow EUC at 140°W (Figure 3b) limits the vertical extent of DCT, and the turbulence below daytime SML does not quickly decay during the restratification period because of the relatively strong shear below SML. Our simulation suggests that the separation of DCT from SML is more prominent in the regions with a deep extending shear layer associated with EUC. In these regions, the turbulence below SML could quickly decay during the restratification in the upper ocean while notable turbulence remains in the strong shear layer below.

DCT can also occur in the off-equatorial regions (Hebert et al., 1991), which is found in the simulation (Figures 3c1–3c4 and 3e1–3e4). Its variability depends on the vertical shear distribution across the equator determined by the relative position and strength of surface zonal currents and EUC. The strongest DCT is seen right above the EUC where shear is the strongest. DCT could penetrate into deeper area off the equator in the vicinity of the EUC. For instance, the deepest DCT is found at 1°S at 170°W (Figure 3c4) and 1.5°N at 140°W (Figure 3e4) where relatively strong shear is found in deeper areas. In addition, DCT can occur in off-equatorial regions without the vertical shear associated with EUC (i.e., near 3°N in Figure 3e3). In these regions, the shear associated with surface currents provides the main energy source of DCT. This is similar to the DCT associated with the MJO-induced surface currents found in the equatorial Indian Ocean (Figure 1c).

3.3.2. Equatorial Atlantic

The thermocline is generally shallower in the equatorial Atlantic than in the equatorial Pacific. Also, the EUC is weaker than that in the Pacific. These different upper ocean structures of velocity and temperature may influence the characteristics of DCT in the Atlantic Ocean. To describe zonal and meridional variations of DCT in the Atlantic, the composite diurnal cycle during the same period is constructed, and is shown along the equator at 2:00, 8:00, 14:00, and 20:00 GMT (Figures 4a1–4a4).

The upper flank of EUC in the western Atlantic is about 30 m deeper than that in the east, and the upward slope is found mostly between 25°W and 4°W (Figure 4b). The westward surface currents are stronger toward the east. The velocity field is smoother than that in the Pacific as TIW activity is weak during this period. West of 10°W, strong vertical shear layer deepens mostly following the depth of the upper flank of EUC as in the Pacific case. DCT with notable penetration below SML is found in most parts of the equatorial Atlantic (44–10°W) including western Atlantic, where the relatively strong vertical shear associated with EUC is evident (Figures S5a1–S5a4). In contrast to the equatorial Pacific where relatively weak DCT exists around the date line, strong DCT (ε~10^{-6} m^2 s^{-3}) is found in most areas of equatorial Atlantic due to a shallower EUC which can produce stronger shear.

Overall diurnal evolution of DCT in equatorial Atlantic is similar to that in the equatorial Pacific. Intensified turbulence layer around the SML base is seen at 20:00 GMT (Figure 4a4) and deepens 2:00–8:00 GMT (Figures 4a1 and 4a2) as in the Pacific case. The separation of DCT from SML in western Atlantic is not

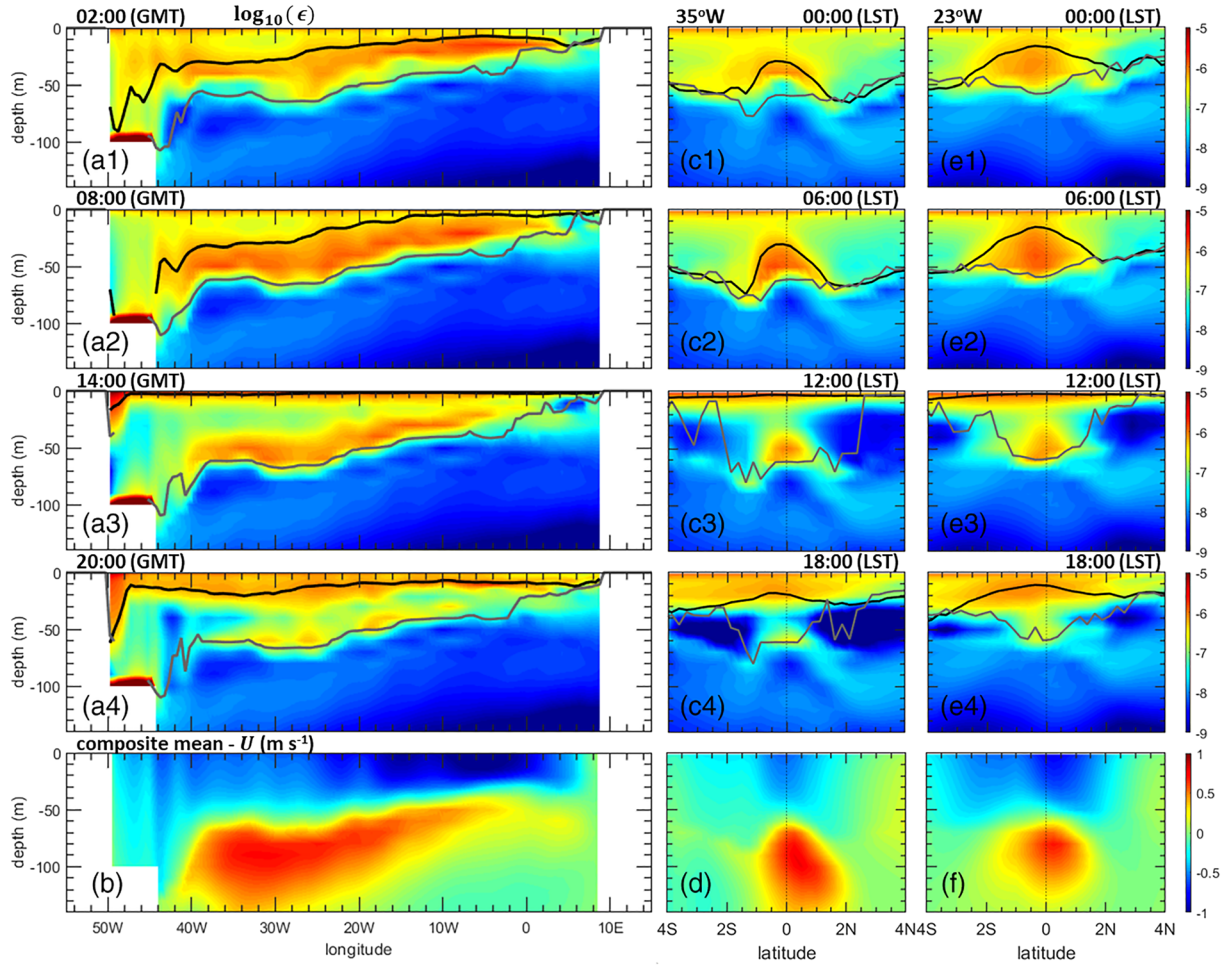

Figure 4. Same as Figure 3 except for equatorial Atlantic (a1–a4) along the equator, (c1–c4) at 35°W between 4°S and 4°N, and (e1–e4) at 23°W between 4°S and 4°N at 02:00, 08:00, 14:00, and 20:00 GMT, respectively. The corresponding local solar time (LST) at 35°W and 23°W is shown. (Note that both locations are in the same time zone. However, time at 35°W lags that at 23°W by about 1 hr.) Variations of *Ri* and SST are shown in Figure S5 in the supporting information.

as prominent as in the central Pacific due to a shallower EUC. The meridional extent of DCT is mostly confined between 2°S and 2°N. The DCT at 23°W extends farther south compared to at western Atlantic 35°W (Figures 4e2 and 4c2) due to the broader westward South Equatorial Current during this period (Figure 4f). It should be noted that the surface current structure changes on a variety of time scales, and thus, the meridional structure of DCT during other periods might be different from that in the present simulation.

4. Conclusions and Discussion

DCT is turbulence associated with the mean current vertical shear in a stratified layer below the SML, and it has often been observed in the eastern equatorial Pacific and Atlantic Oceans. Since mixing in the upper ocean in these regions may largely influence SST variability (e.g., Moum et al., 2009, 2013), a proper representation of vertical mixing in the OGCM is crucial for the accurate simulation of SST in the tropical Oceans (e.g., Jia et al., 2015). As most of state-of-the-art global climate models have longstanding SST bias in the cold tongue region (e.g., Zheng et al., 2012), a parameterization that adequately represents the vertical mixing associated with DCT in the cold tongue region may reduce SST biases and in turn improve prediction of climate variability (e.g., Warner & Moum, 2019). However, the simulation of DCT in a global OGCM has not been explicitly demonstrated so far, and thus, the model's ability to simulate DCT is still unknown.

We present the first simulation of DCT by a global OGCM. The model is integrated with hourly atmospheric forcing derived from reanalysis products. A k-ε model based second-moment turbulence closure is used to parameterize vertical mixing, and thus, TKE dissipation rate ε computed during the model integration can be directly compared with in situ microstructure observations. The model is able to reproduce observed structures of DCT very well. The MI state has been well reproduced in all three equatorial ocean basins. Also, the intensity of DCT has been well reproduced. In addition, processes which modulate the simulated DCT in the eastern Pacific such as the influence of TIWs are consistent with results from previous observational studies.

Large-scale spatial variations of DCT are fully described by the analysis of model simulation. The analysis demonstrates the large zonal extent of DCT over the central and eastern equatorial Pacific, which spans 170°E to 105°W. Also, DCT is evident in most areas in the equatorial Atlantic. The depth of turbulence penetration is mostly controlled by the depth of the upper flank of EUC. In addition, DCT exists in off-equatorial regions away from EUC where the vertical shear is associated with surface currents.

A composite diurnal variation of TKE dissipation is constructed to investigate the evolution of DCT at each location. When the nighttime cooling starts, a strong turbulence layer is found right above the base of SML. It continues to deepen beyond the base of SML and penetrates into the maximum shear region around the upper flank of EUC. The turbulence below SML decays during the upper ocean restratification caused by daytime warming. In the central equatorial Pacific around the dateline, the separation of DCT layer from SML is much more prominent during restratification than other areas. This DCT layer is located at the upper flank of EUC, which is very deep in the central equatorial Pacific. In this region, the turbulence in the layer of weak shear and stratification right below the SML quickly decays during restratification.

While this study demonstrated the capability of simulating DCT by a global OGCM, and described the large-scale variability of DCT in the entire equatorial oceans, the model results can be validated for only limited areas such as 140°W in the eastern equatorial Pacific. Therefore, it is necessary to verify large-scale spatial variations of DCT found in the model simulation by future observations. Observations of DCT in the broader region in three equatorial ocean basins are needed to confirm the simulation results. For example, the prominent separation of DCT layer from the SML in the central Pacific could be identified by microstructure measurements. Also, DCT in the equatorial Indian Ocean was measured only at one location for a specific period. Since the major equatorial current system in the Indian Ocean varies on the seasonal time scale because of the monsoon, it is expected that characteristics of DCT changes substantially in time and space. Further observational and modeling studies are necessary to address these issues.

Data Availability Statement

The CFSR data can be found online (at https://www.ncdc.noaa.gov/data-access/model-data/model-datasets/climate-forecast-system-version2-cfsv2). The MERRA data can be found at the website (https://disc.gsfc.nasa.gov/datasets/MAT1NXOCN_5.2.0/summary?keywords=merra). In situ mooring data are obtained from TAO, PIRATA, and RAMA mooring sites available online (at https://www.pmel.noaa.gov/gtmba/).Computing resources were partly provided by the HPC system at the Texas A&M University (College Station and Corpus Christi) and the Climate Simulation Laboratory at NCAR's Computational and Information Systems Laboratory.

Acknowledgments
We would like to thank Alexander Soloviev for insightful discussions. We thank the three anonymous reviewers for their insightful comments and suggestions. This research is supported by NOAA Grants NA15OAR431074 and NA17OAR4310256. T. S. and S. P. are also supported by DOD Grant W911NF-20-1-0309. T. S. is also supported by NSF Grant OCE-1658218 and NASA Grant NNX17AH25G.

References

Brandt, P., Funk, A., Tantet, A., Johns, W. E., & Fischer, J. (2014). The Equatorial Undercurrent in the central Atlantic and its relation to tropical Atlantic variability. *Climate Dynamics*, *43*(11), 2985–2997. https://doi.org/10.1007/s00382-014-2061-4

Burchard, H., & Bolding, K. (2001). Comparative analysis of four second-moment turbulence closure models for the oceanic mixed layer. *Journal of Physical Oceanography*, *31*(8), 1943–1968. https://doi.org/10.1175/1520-0485(2001)031<1943:CAOFSM>2.0.CO;2

Burchard, H., Bolding, K., & Villarreal, M. R. (1999). *GOTM, a General Ocean Turbulence Model. Theory, implementation and test cases.* Tech. Rep. EUR 18745 EN, European Commission, Ispra, Italy.

Canuto, V. M., Howard, A., Cheng, Y., & Dubovikov, M. S. (2001). Ocean turbulence. Part I: One-point closure model—Momentum and heat vertical diffusivities. *Journal of Physical Oceanography*, *31*, 1413–1426.https://doi.org/10.1175/1520-0485(2001)031<1413:OTPIOP>2.0.CO;2

Clayson, C. A., & Kantha, L. H. (1999). Turbulent kinetic energy and its dissipation rate in the equatorial mixed layer. *Journal of Physical Oceanography*, *29*(9), 2146–2166. https://doi.org/10.1175/1520-0485(1999)029<2146:TKEAID>2.0.CO;2

de Szoeke, S. P., & Xie, S.-P. (2008). The tropical eastern Pacific seasonal cycle: Assessment of errors and mechanisms in IPCC AR4 coupled ocean–atmosphere general circulation models. *Journal of Climate*, *21*(11), 2573–2590. https://doi.org/10.1175/2007JCLI1975.1

Edson, J. B., Jampana, V., Weller, R. A., Bigorre, S. P., Plueddemann, A. J., Fairall, C. W., et al. (2013). On the exchange of momentum over the open ocean. *Journal of Physical Oceanography*, *43*(8), 1589–1610. https://doi.org/10.1175/JPO-D-12-0173.1

Fairall, C. W., Bradley, E. F., Hare, J. E., Grachev, A. A., & Edson, J. B. (2003). Bulk parameterization of air-sea fluxes: Updates and verification for the COARE algorithm. *Journal of Climate*, *16*(4), 571–591. https://doi.org/10.1175/1520-0442(2003)016<0571:BPOASF>2.0.CO;2

Foltz, G. R., Schmid, C., & Lumpkin, R. (2018). An enhanced PIRATA dataset for tropical Atlantic Ocean-atmosphere research. *Journal of Climate*, *31*(4), 1499–1524. https://doi.org/10.1175/JCLI-D-16-0816.1

Ge, X., Wang, W., Kumar, A., & Zhang, Y. (2017). Importance of the vertical resolution in simulating SST diurnal and intraseasonal variability in an oceanic general circulation model. *Journal of Climate*, *30*(11), 3963–3978. https://doi.org/10.1175/JCLI-D-16-0689.1

Giarolla, E., Nobre, P., Malagutti, M., & Pezzi, L. P. (2005). The Atlantic Equatorial Undercurrent: PIRATA observations and simulations with GFDL Modular Ocean Model at CPTEC. *Geophysical Research Letters*, *32*, L10617. https://doi.org/10.1029/2004GL022206

Gregg, M. C., Peters, H., Wesson, J. C., Oakey, N. S., & Shay, T. J. (1985). Intensive measurements of turbulence and shear in the equatorial undercurrent. *Nature*, *318*(6042), 140–144. https://doi.org/10.1038/318140a0

Griffies, S. M. (2012). Elements of the Modular Ocean Model (MOM): 2012 Release. GFDL Ocean Group Technical Report No. 7, Princeton, NJ.

Hebert, D., Moum, J. N., & Caldwell, D. R. (1991). Does ocean turbulence peak at the equator?: Revisited. *Journal of Physical Oceanography*, *21*(11), 1690–1698. https://doi.org/10.1175/1520-0485(1991)021<1690:DOTPAT>2.0.CO;2

Holmes, R. M., & Thomas, L. N. (2015). The modulation of equatorial turbulence by tropical instability waves in a Regional Ocean Model. *Journal of Physical Oceanography*, *45*(4), 1155–1173. https://doi.org/10.1175/JPO-D-14-0209.1

Huang, P., Xie, S.-P., Hu, K., Huang, G., & Huang, R. (2013). Patterns of the seasonal response of tropical rainfall to global warming. *Nature Geoscience*, *6*(5), 357–361. https://doi.org/10.1038/ngeo1792

Hummels, R., Dengler, M., & Bourlès, B. (2013). Seasonal and regional variability of upper ocean diapycnal heat flux in the Atlantic cold tongue. *Progress in Oceanography*, *111*, 52–74. https://doi.org/10.1016/j.pocean.2012.11.001

Inoue, R., Lien, R.-C., & Moum, J. N. (2012). Modulation of equatorial turbulence by a tropical instability wave. *Journal of Geophysical Research*, *117*, C10009. https://doi.org/10.1029/2011JC007767

Inoue, R., Lien, R.-C., Moum, J. N., Perez, R. C., & Gregg, M. C. (2019). Variations of equatorial shear, stratification, and turbulence within a tropical instability wave cycle. *Journal of Geophysical Research: Oceans*, *124*, 1858–1875. https://doi.org/10.1029/2018JC014480

Jia, Y., Furue, R., & McCreary, J. P. (2015). Impacts of regional mixing on the temperature structure of the equatorial Pacific Ocean. Part 2: Depth-dependent vertical diffusion. *Ocean Modelling*, *91*, 112–127. https://doi.org/10.1016/j.ocemod.2015.02.007

Kosaka, Y., & Xie, S.-P. (2013). Recent global-warming hiatus tied to equatorial Pacific surface cooling. *Nature*, *501*(7467), 403–407. https://doi.org/10.1038/nature12534

Large, W. G., McWilliams, J. C., & Doney, S. C. (1994). Oceanic vertical mixing: A review and a model with nonlocal boundary layer parameterization. *Reviews of Geophysics*, *32*(4), 363–403. https://doi.org/10.1029/94RG01872

Li, G., & Xie, S.-P. (2014). Tropical biases in CMIP5 multimodel ensemble: The excessive equatorial Pacific cold tongue and double ITCZ problems. *Journal of Climate*, *27*(4), 1765–1780. https://doi.org/10.1175/JCLI-D-13-00337.1

Lien, R.-C., Caldwell, D. R., Gregg, M. C., & Moum, J. N. (1995). Turbulence variability at the equator in the central Pacific at the beginning of the 1991-1993 El Niño. *Journal of Geophysical Research*, *100*(C4), 6881–6898. https://doi.org/10.1029/94JC03312

Lien, R.-C., D'Asaro, E., & Menkes, C. (2008). Modulation of equatorial turbulence by tropical instability waves. *Geophysical Research Letters*, *35*, L24607. https://doi.org/10.1029/2008GL035860

Lien, R.-C., McPhaden, M. J., & Gregg, M. C. (1996). High-frequency internal waves at 0°, 140°W and their possible relationship to deep-cycle turbulence. *Journal of Physical Oceanography*, *26*(4), 581–600. https://doi.org/10.1175/1520-0485(1996)026<0581:HFIWAA>2.0.CO;2

Lyman, J. M., Johnson, G. C., & Kessler, W. S. (2007). Distinct 17- and 33-day tropical instability waves in subsurface observations. *Journal of Physical Oceanography*, *37*(4), 855–872. https://doi.org/10.1175/JPO3023.1

McPhaden, M. J., Busalacchi, A. J., Cheney, R., Donguy, J.-R., Gage, K. S., Halpern, D., et al. (1998). The Tropical Ocean-Global Atmosphere observing system: A decade of progress. *Journal of Geophysical Research*, *103*(C7), 14,169–14,240. https://doi.org/10.1029/97JC02906

McPhaden, M. J., Meyers, G., Ando, K., Masumoto, Y., Murty, V. S., Ravichandran, M., et al. (2009). RAMA: The Research Moored Array for African-Asian-Australian monsoon analysis and prediction. *Bulletin of the American Meteorological Society*, *90*(4), 459–480. https://doi.org/10.1175/2008BAMS2608.1

Moum, J. N., & Caldwell, D. R. (1985). Local influences on shear-flow turbulence in the equatorial ocean. *Science*, *230*(4723), 315–316. https://doi.org/10.1126/science.230.4723.315

Moum, J. N., Caldwell, D. R., & Paulson, C. A. (1989). Mixing in the equatorial surface layer and thermocline. *Journal of Geophysical Research*, *94*(C2), 2005–2022. https://doi.org/10.1029/JC094iC02p02005

Moum, J. N., de Szoeke, S. P., Smyth, W. D., Edson, J. B., DeWitt, H. L., Moulin, A. J., et al. (2014). Air-sea interactions from westerly wind bursts during the November 2011 MJO in the Indian Ocean. *Bulletin of the American Meteorological Society*, *95*(8), 1185–1199. https://doi.org/10.1175/BAMS-D-12-00225.1

Moum, J. N., Hebert, D., Paulson, C. A., & Caldwel, D. R. (1992). Turbulence and internal waves at the equator Part I: Statistics from towed thermistors and a microstructure profiler. *Journal of Physical Oceanography*, *22*(11), 1330–1345. https://doi.org/10.1175/1520-0485(1992)022<1330:TAIWAT>2.0.CO;2

Moum, J. N., Lien, R.-C., Perlin, A., Nash, J. D., Gregg, M. C., & Wiles, P. J. (2009). Sea surface cooling at the equator by subsurface mixing in tropical instability waves. *Nature Geoscience*, *2*(11), 761–765. https://doi.org/10.1038/ngeo657

Moum, J. N., Perlin, A., Nash, J. D., & McPhaden, M. J. (2013). Seasonal sea surface cooling in the equatorial Pacific cold tongue controlled by ocean mixing. *Nature*, *500*(7460), 64–67. https://doi.org/10.1038/nature12363

Peters, H., Gregg, M. C., & Toole, J. M. (1988). On the parameterization of equatorial turbulence. *Journal of Geophysical Research*, *93*(C2), 1199. https://doi.org/10.1029/JC093iC02p01199

Pham, H. T., Sarkar, S., & Winters, K. B. (2012). Near-N oscillations and deep-cycle turbulence in an upper-Equatorial Undercurrent model. *Journal of Physical Oceanography*, *42*(12), 2169–2184. https://doi.org/10.1175/JPO-D-11-0233.1

Pham, H. T., Sarkar, S., & Winters, K. B. (2013). Large-eddy simulation of deep-cycle turbulence in an Equatorial Undercurrent model. *Journal of Physical Oceanography*, *43*(11), 2490–2502. https://doi.org/10.1175/JPO-D-13-016.1

Pham, H. T., Smyth, W. D., Sarkar, S., & Moum, J. N. (2017). Seasonality of deep cycle turbulence in the eastern equatorial Pacific. *Journal of Physical Oceanography*, *47*(9), 2189–2209. https://doi.org/10.1175/JPO-D-17-0008.1

Pujiana, K., Moum, J. N., & Smyth, W. D. (2018). The role of turbulence in redistributing upper-ocean heat, freshwater, and momentum in response to the MJO in the equatorial Indian Ocean. *Journal of Physical Oceanography*, *48*(1), 197–220. https://doi.org/10.1175/JPO-D-17-0146.1

Richter, I., Doi, T., Chang, P., Xu, Z., Kataoka, T., Tozuka, T., et al. (2016). An overview of coupled GCM biases in the tropics. In S. K. Behera, & T. Yamagata (Eds.), *Indo-Pacific climate variability and predictability* (pp. 213–263). Texas: World Scientific. https://doi.org/10.1142/9789814696623_0008

Rienecker, M. M., Suarez, M. J., Gelaro, R., Todling, R., Bacmeister, J., Liu, E., et al. (2011). MERRA: NASA's Modern-Era Retrospective Analysis for Research and Applications. *Journal of Climate*, *24*(14), 3624–3648. https://doi.org/10.1175/JCLI-D-11-00015.1

Rodi, W. (1987). Examples of calculation methods for flow and mixing in stratified fluids. *Journal of Geophysical Research*, *92*(C5), 5305–5328. https://doi.org/10.1029/JC092iC05p05305

Saha, S., Moorthi, S., Pan, H.-L., Wu, X., Wang, J., Nadiga, S., et al. (2010). The NCEP Climate Forecast System Reanalysis. *Bulletin of the American Meteorological Society*, *91*(8), 1015–1058. https://doi.org/10.1175/2010BAMS3001.1

Samanta, D., Karnauskas, K. B., & Goodkin, N. F. (2019). Tropical Pacific SST and ITCZ biases in climate models: Double trouble for future rainfall projections? *Geophysical Research Letters*, *46*, 2242–2252. https://doi.org/10.1029/2018GL081363

Schudlich, R. R., & Price, J. F. (1992). Diurnal cycles of current, temperature, and turbulent dissipation in a model of the equatorial upper ocean. *Journal of Geophysical Research*, *97*(C4), 5409–5422. https://doi.org/10.1029/91JC01918

Shinoda, T. (2010). Observed dispersion relation of Yanai waves and 17-day tropical instability waves in the Pacific Ocean. *SOLA*, *6*, 17–20. https://doi.org/10.2151/sola.2010-005

Shinoda, T. (2012). Observation of first and second baroclinic mode Yanai waves in the ocean. *Quarterly Journal of the Royal Meteorological Society*, *138*(665), 1018–1024. https://doi.org/10.1002/qj.968

Smyth, W. D., & Moum, J. N. (2013). Marginal instability and deep cycle turbulence in the eastern equatorial Pacific Ocean. *Geophysical Research Letters*, *40*, 6181–6185. https://doi.org/10.1002/2013GL058403

Smyth, W. D., Moum, J. N., Li, L., & Thorpe, S. A. (2013). Diurnal shear instability, the descent of the surface shear layer, and the deep cycle of equatorial turbulence. *Journal of Physical Oceanography*, *43*(11), 2432–2455. https://doi.org/10.1175/JPO-D-13-089.1

Smyth, W. D., Nash, J. D., & Moum, J. N. (2019). Self-organized criticality in geophysical turbulence. *Scientific Reports*, *9*(1), 3747. https://doi.org/10.1038/s41598-019-39869-w

Smyth, W. D., Pham, H. T., Moum, J. N., & Sakar, S. (2017). Pulsating turbulence in a marginally unstable stratified shearflow. *Journal of Fluid Mechanics*, *822*, 327–341. https://doi.org/10.1017/jfm.2017.283

Thorpe, S. A., & Liu, Z. (2009). Marginal instability? *Journal of Physical Oceanography*, *39*(9), 2373–2381. https://doi.org/10.1175/2009JPO4153.1

Umlauf, L., Burchard, H., & Bolding, K. (2005). *GOTM—Scientific Documentation. Version 3.2*. Tech. Rep. 63, Leibniz-Institute for Baltic Sea Research, Warnemunde, Germany.

Wang, D., McWilliams, J. C., & Large, W. G. (1998). Large-eddy simulation of the diurnal cycle of deep equatorial turbulence. *Journal of Physical Oceanography*, *28*(1), 129–148. https://doi.org/10.1175/1520-0485(1998)028<0129:LESOTD>2.0.CO;2

Warner, S. J., & Moum, J. N. (2019). Feedback of mixing to ENSO phase change. *Geophysical Research Letters*, *43*, 13,920–13,927. https://doi.org/10.1029/2019GL085415

Wenegrat, J. O., & McPhaden, M. J. (2015). Dynamics of the surface layer diurnal cycle in the equatorial Atlantic Ocean (0°, 23°W). *Journal of Geophysical Research: Oceans*, *120*, 563–581. https://doi.org/10.1002/2014JC010504

Xie, S.-P. (2013). Unequal equinoxes. *Nature*, *500*(7460), 33–34. https://doi.org/10.1038/nature12456

Zheng, Y., Lin, J.-L., & Shinoda, T. (2012). The equatorial Pacific cold tongue simulated by IPCC AR4 coupled GCMs: Upper ocean heat budget and feedback analysis. *Journal of Geophysical Research*, *117*, C05024. https://doi.org/10.1029/2011JC007746